MIMO DETECTION IN SINGLE CARRIER SYSTEMS

Johanna Ketonen, Juha Karjalainen†, Markku Juntti and Tuomo Hänninen

Centre for Wireless Communications
University of Oulu
P.O. Box 4500, 90014, Oulu, Finland
{johannak}{markku.juntti}{tuomo.hanninen}@ee.oulu.fi

†Renesas Mobile Europe Ltd.
Elektroniikkatie 13, Oulu, Finland
Juha.Karjalainen@renesasmobile.com

ABSTRACT

This paper proposes a novel 2-stage receiver for single user single-carrier frequency-division multiple access (SC-FDMA) uplink transmission. The proposed receiver consists of separate stages for inter-symbol interference (ISI) and inter-antenna interference (IAI) mitigation in frequency selective MIMO channels. The main focus is on the single user case where the IAI between the MIMO streams needs to be addressed. A new 2-stage receiver structure is introduced where sphere detection algorithms are used in the time domain to remove the IAI while minimum mean square error (MMSE) equalization is used in the frequency domain to suppress the ISI. The numerical results show that the proposed receiver outperforms the conventional MMSE receiver under the presence of spatial correlation between both the transmit and receive antennas.

1. INTRODUCTION

Single-carrier frequency-division multiple access (SC-FDMA) has been adopted in the third generation partnership project (3GPP) long term evolution (LTE) as the uplink transmission scheme. Lately, the combination of multiple-input multiple-output (MIMO) and SC-FDMA has been considered for the LTE advanced (LTE-A) uplink [1] in order to increase the transmission rates. SC-FDMA has been selected in the uplink instead of orthogonal frequency division multiplexing (OFDM) because of its reduced peak-to-average power ratio which lowers the transmitter cost in the form of cheaper power amplifier [2].

In response to the demand for higher data rates, the LTE-A standard specifies up to 4 transmit antennas in the user terminal. This motivates the study of more advanced receivers for combating the inter-antenna interference (IAI) and the inter-symbol interference (ISI). During the last decade, frequency domain (FD) minimum mean square error (MMSE) equalization and MMSE based turbo equalization have been studied extensively for single carrier transmission [3], [4], [5]. Sphere detectors (SD) calculate the maximum likelihood solution with reduced complexity [6] and the list sphere detector (LSD) [7] approximates the maximum *a posteriori* probability (MAP) detector producing soft outputs for the channel decoder. Sphere detectors and other tree search algorithms for MIMO detection have been studied mainly for the downlink or in the MIMO-OFDM context [8], [9].

In this paper, we consider a 2-stage receiver structure for a single carrier MIMO system. The idea of the proposed structure is to separate the mitigation of ISI and IAI into separate stages. Linear FD MMSE based equalization is used to suppress the ISI. IAI cancellation is carried out at a non-linear detector, e.g., a sphere detector. The MMSE filter can be seen as a channel shortening filter. As a result, the complexity of the sphere detector can be reduced. Two different sphere detection algorithms are considered, namely the K-best [10] and the selective spanning with fast enumeration (SSFE) [11]. We compare the frame error rate (FER) performance of the proposed method to that of the traditional FD MMSE filter with soft demodulation and the soft cancellation MMSE (SC-MMSE) turbo equalizer. Furthermore, we provide complexity comparisons of the proposed and traditional structures.

This research was done in the CoMIT project which was supported by Elektrobit, Nokia, Nokia Siemens Networks, Xilinx and the Finnish Funding Agency for Technology and Innovation (Tekes).

2. SYSTEM MODEL

A single carrier based vertically encoded BLAST MIMO transmission system with T transmit (TX) and R receive (RX) antennas is considered in this paper. The system model is presented in Figure 1. The encoded data stream is interleaved and modulated into symbols. After the parallel-to-serial conversion, a cyclic prefix (CP) is added. At the receiver, a K-point DFT is performed and the symbols from the allocated carriers are selected. After the frequency domain equalization, the symbols are transformed into time domain and the detector is used to calculate the bit log-likelihood ratios (LLR) for the decoder.

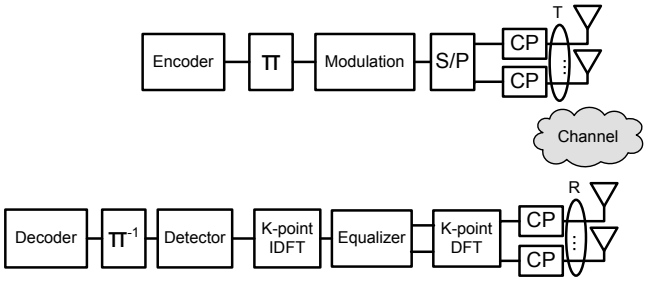

Figure 1: The vertically encoded single carrier MIMO system model.

After CP removal, the received signal vector $\mathbf{r} \in \mathbb{C}^{RK}$ can be expressed as

$$\mathbf{r} = \mathbf{H}\mathbf{x} + \mathbf{v}, \tag{1}$$

where $\mathbf{v} \in \mathbb{C}^{RK}$ is independent and identically distributed complex Gaussian noise with variance σ^2, $\mathbf{x} \in \mathbb{C}^{TK}$ is the transmitted signal, $\mathbf{H} \in \mathbb{C}^{RK \times TK}$ is the circulant block channel matrix and K is the length of the DFT. The channel matrix

$\mathbf{H}$ can be written as

$$\begin{bmatrix} \mathbf{H}^{1,1} & \dots & \mathbf{H}^{1,T} \\ \vdots & \dots & \vdots \\ \mathbf{H}^{R,1} & \dots & \mathbf{H}^{R,T} \end{bmatrix},$$

where $\mathbf{H}^{r,t} \in \mathbb{C}^{K\times K}$ is a channel submatrix between tth TX and rth RX antenna.

3. 2-STAGE MIMO RECEIVERS

3.1 Frequency Domain MMSE Filter with Sphere Detection

The MMSE filter is used to suppress the ISI. It also acts as a channel shortening filter, producing a shortened channel matrix for the sphere detector. The sphere detector is used for MIMO detection, i.e, removing the interference between the MIMO streams. The receiver structure for vertically encoded $R \times T$ MIMO is illustrated in Figure 2.

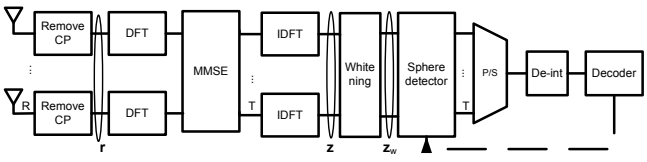

Figure 2: Receiver with sphere detection.

3.1.1 MMSE filter

The coefficients of the MMSE filter are derived to suppress ISI and the filter coefficients $\mathbf{\Omega} \in \mathbb{C}^{RK\times RK}$ can be determined according to the MMSE criterion

$$\mathbf{\Omega} = \min_{\mathbf{\Omega}} \underbrace{\mathrm{tr}\{E_{\mathbf{x},\mathbf{v}}\{(\mathbf{F}_R^{-1}\mathbf{\Omega}^{\mathrm{H}}\mathbf{F}_R\mathbf{r} - \tilde{\mathbf{H}}\mathbf{x})(\mathbf{F}_R^{-1}\mathbf{\Omega}^{\mathrm{H}}\mathbf{F}_R\mathbf{r} - \tilde{\mathbf{H}}\mathbf{x})^{\mathrm{H}}\}\}}_{\mathbf{e}}, \quad (2)$$

where $\mathbf{e}$ is the mean square error (MSE), the expectation $E\{\cdot\}$ is respect to $\mathbf{x}$ and $\mathbf{v}$, $\tilde{\mathbf{H}} \in \mathbb{C}^{RK\times TK}$ is the target channel matrix and it consists of submatrices $\mathrm{diag}(\mathbf{H}^{r,t})$, i.e, the diagonal elements (1st channel taps) from $\mathbf{H}^{r,t}$, $\mathbf{F}_R \in \mathbb{C}^{RK\times RK}$ is a block diagonal DFT matrix $\mathbf{I}_R \otimes \mathbf{F}_K$, $\mathbf{F}_K$ is the DFT matrix, $\mathrm{tr}\{\cdot\}$ is the matrix trace operator and $\otimes$ is the Kronecker product. Assuming $E\{\mathbf{v}\mathbf{v}^{\mathrm{H}}\} = \sigma^2\mathbf{I}_{RK}$, $E\{\mathbf{x}\mathbf{x}^{\mathrm{H}}\} = \mathbf{I}_{TK}$, $E\{\mathbf{x}\mathbf{v}^{\mathrm{H}}\} = \mathbf{0}_{TK\times RK}$ and $\mathbf{F}_R\mathbf{F}_R^{-1} = \mathbf{I}$, the MSE given by (2) can be rewritten as

$$\begin{aligned} \mathbf{e} &= TK - \mathrm{tr}\{\mathbf{\Omega}^{\mathrm{H}}\mathbf{\Gamma}\tilde{\mathbf{\Gamma}}^{\mathrm{H}}\} \\ &\quad -\mathrm{tr}\{\tilde{\mathbf{\Gamma}}\mathbf{\Gamma}^{\mathrm{H}}\mathbf{\Omega}\} + \mathrm{tr}\{\mathbf{\Omega}^{\mathrm{H}}\mathbf{\Sigma}_r\mathbf{\Omega}\}. \end{aligned} \quad (3)$$

Since (3) is convex respect to $\mathbf{\Omega}^{\mathrm{H}}$, the optimal MMSE filtering matrix that minimizes the MSE can be found from $(\partial\mathbf{e})/(\partial\mathbf{\Omega}^{\mathrm{H}}) = 0$. Thus, the optimal MMSE filtering matrix can be expressed as

$$\mathbf{\Omega} = \mathbf{\Sigma}_r^{-1}\mathbf{\Gamma}\tilde{\mathbf{\Gamma}}^{\mathrm{H}}, \quad (4)$$

where $\mathbf{\Sigma}_r = \mathbf{\Gamma}\mathbf{\Gamma}^{\mathrm{H}} + \sigma^2\mathbf{I} \in \mathbb{C}^{RK\times RK}$, $\mathbf{I} \in \mathbb{R}^{RK\times RK}$ is an identity matrix and the frequency domain channel matrix $\mathbf{\Gamma} = \mathbf{F}_R\mathbf{H}\mathbf{F}_T^{-1} \in \mathbb{C}^{RK\times TK}$. The (i,j) term of the equivalent channel $\mathbf{\Phi} \in \mathbb{C}^{R\times T}$ can be calculated as

$$\varphi_{i,j} = \frac{1}{K}\mathrm{tr}((\tilde{\mathbf{\Gamma}}\mathbf{\Gamma}^{\mathrm{H}}\mathbf{\Sigma}_r^{-1}\mathbf{\Gamma})_{i,j}) \quad (5)$$

where $i = 1,...,R$ and $j = 1,...,T$ and the (i,j) term of the variance of residual interference $\mathbf{\Sigma}_w \in \mathbb{C}^{R\times T}$ as

$$\sigma_{i,j}^2 = \frac{1}{K}\mathrm{tr}((\tilde{\mathbf{\Gamma}}\mathbf{\Gamma}^{\mathrm{H}}\mathbf{\Omega})_{i,j}) - \frac{1}{K}\mathrm{tr}((\mathbf{\Omega}^{\mathrm{H}}\mathbf{\Gamma}\mathbf{\Gamma}^{\mathrm{H}}\mathbf{\Omega})_{i,j}). \quad (6)$$

The equalized signal $\mathbf{z} \in \mathbb{C}^{RK}$ after the IDFT, can be written as

$$\mathbf{z} = \mathbf{F}_R^{-1}\mathbf{\Omega}^{\mathrm{H}}\mathbf{F}_R\mathbf{r}. \quad (7)$$

After the frequency domain filtering, the noise is not white and has the variance matrix $\mathbf{\Sigma}_w$ from (6). The likelihood function term $1/\sigma^2||\mathbf{z} - \mathbf{\Phi}\mathbf{s}||_2^2$ then becomes $\mathbf{\Sigma}_w^{-1/2}||\mathbf{z} - \mathbf{\Phi}\mathbf{s}||_2^2$, where $\mathbf{s}$ is a possible transmitted symbol vector. The variance of residual interference can be taken into account either by whitening the noise or including it in the distance calculations. The whitening can be done by multiplying $\mathbf{z}$ and $\mathbf{\Phi}$ with the inverse square root of the variance matrix $\mathbf{\Sigma}_w$, i.e, $\mathbf{z}_w = \mathbf{\Sigma}_w^{-1/2}\mathbf{z}$ and $\mathbf{\Phi}_w = \mathbf{\Sigma}_w^{-1/2}\mathbf{\Phi}$. The inverse square root can be obtained from $\mathbf{\Sigma}_w^{1/2} = \mathrm{chol}(\mathbf{\Sigma}_w)$ or $\mathbf{\Sigma}_w^{1/2} = \mathbf{U}\Lambda^{1/2}$, when $\mathbf{\Sigma}_w = \mathbf{U}\mathbf{\Lambda}\mathbf{U}^{\mathrm{H}}$ and $\mathbf{\Lambda}$ contains the eigenvalues and $\mathbf{U}$ contains the eigenvectors of $\mathbf{\Sigma}_w$.

3.1.2 Sphere detector

The structure of the sphere detector is presented in Figure 3. In the QRD block, QR decomposition $\mathbf{\Phi}_\mathbf{w} = \mathbf{Q}\mathbf{R}$ of the whitened channel matrix is performed where $\mathbf{Q} \in \mathbb{C}^{R\times R}$ and $\mathbf{R} \in \mathbb{C}^{T\times R}$. The QRD is performed only once in a block since the channel matrix $\mathbf{\Phi}$ is invariant, i.e, it is common for all symbol vectors in $\mathbf{z}$. Each symbol vector $\mathbf{z}_{w_{[n]}} \in \mathbb{C}^T$ from the whitened vector $\mathbf{z}_w$ is multiplied with matrix $\mathbf{Q}$ from QRD as $\mathbf{z}'_{w_{[n]}} = \mathbf{Q}\mathbf{z}_{w_{[n]}}$. The tree search is then performed separately for each whitened symbol vector.

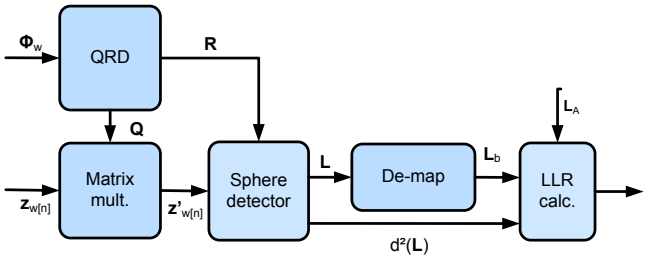

Figure 3: The sphere detector structure.

The squared partial Euclidean distance (PED) of $\mathbf{s}_i^T$, i.e., the square of the distance between the partial candidate symbol vector and the partial received vector, can be calculated in the sphere detector block as

$$d(\mathbf{s}_i^T) = \sum_{j=i}^{T}\left|\mathbf{z}'_{w_{[n]_j}} - \sum_{l=j}^{T}R_{j,l}s_l\right|^2, \quad (8)$$

where $i = T\ldots,1$ and $\mathbf{s}_i^T$ denotes the last $T-i+1$ components of vector $\mathbf{s}$ [6].

The resulting list of candidate symbol vectors $\mathscr{L}$ is demapped into binary form and the LLR for the transmitted bit k is calculated as

$$L_{\mathrm{D}}(b_k) = \ln \frac{p(\mathbf{z}_{w_{[n]}}|b_k=+1)}{p(\mathbf{z}_{w_{[n]}}|b_k=-1)}, \tag{9}$$

where

$$p(\mathbf{z}_{w_{[n]}}|b_k=+1) = \sum_{\mathbf{s}\in\Theta, b_k=+1} e^{\frac{-d(\mathbf{s})}{2}} \tag{10}$$

and Θ is the set of possible transmitted symbol vectors. The LLRs can be updated from the decoder feedback L_A as:

$$\hat{L}_D(b_k|\mathbf{z}_{w_{[n]}}) = L_A(b_k) + \ln \frac{\sum_{\mathbf{b}\in\mathscr{L}_{k,+1}} \exp(\Lambda(\mathbf{b},\mathbf{b}_{[k]},\mathbf{l}_{A,[k]}|\mathbf{z}_{w_{[n]}},\mathbf{\Phi_w}))}{\sum_{\mathbf{b}\in\mathscr{L}_{k,-1}} \exp(\Lambda(\mathbf{b},\mathbf{b}_{[k]},\mathbf{l}_{A,[k]}|\mathbf{z}_{w_{[n]}},\mathbf{\Phi_w}))}, \tag{11}$$

where

$$\Lambda(\mathbf{b},\mathbf{b}_{[k]},\mathbf{l}_{A,[k]}|\mathbf{z}_{w_{[n]}},\mathbf{\Phi_w}) = -\frac{1}{2}||\mathbf{z}_{w_{[n]}} - \mathbf{\Phi_w}\mathbf{s}||^2 + \frac{1}{2}\mathbf{b}_{[k]}^T\mathbf{l}_{A,[k]}, \tag{12}$$

$\mathbf{l}_{A,[k]}$ is a vector of L_A and $\mathbf{b}_{[k]}$ is a vector corresponding to k from the transmitted binary vector $\mathbf{b}$.

Two different tree search algorithms are considered in this paper. The K-best algorithm [10] is a breadth-first search based algorithm, which keeps the K nodes which have the smallest accumulated Euclidean distances at each level. If the PED is larger than the squared sphere radius C_0, the corresponding node will not be expanded. We assume no sphere constraint or $C_0 = \infty$, but set the value for the list size K instead, as is common with the K-best algorithms.

The selective spanning with fast enumeration algorithm [11] is characterized by vector $\mathbf{m} = [m_1, ..., m_M]$, which defines the number of spans for each node on level i and also the length of the final candidate list. For example in a real 2×2 antenna and 16-QAM system, the vector $\mathbf{m} = [4,4,4,4]$ would lead to a full search and the length of 256 candidates in the final list. The spanned nodes are never deleted and the number of nodes in the search tree can be determined using vector $\mathbf{m}$ i.e. $\prod_{j=i}^{T} m_j$.

The slicer unit is an essential part of the SSFE algorithm. It selects a set of closest constellation points $\mathbf{s}^i$ such that the PED increment is minimized at each level e.g.,

$$\left\|e_i(\mathbf{s}^i)\right\|^2 = \left\| \underbrace{\mathbf{z}'_{w_{[n]_i}} - \sum_{j=i+1}^{T} R_{i,j}s_j}_{b_{i+1}(\mathbf{s}^{i+1})} - R_{i,i}s_i \right\|^2. \tag{13}$$

Minimizing $\left\|e_i(\mathbf{s}^i)\right\|^2$ is equivalent to the minimization of $\|e_i(\mathbf{s}^i)/R_{ii}\|^2$

$$\left\| \frac{e_i(\mathbf{s}^i)}{R_{ii}} \right\|^2 = \left\| \underbrace{b_{i+1}(\mathbf{s}^{i+1})/R_{ii}}_{\varepsilon} - s_i \right\|^2. \tag{14}$$

Equation (14) is essential for the slicer unit which selects the closest constellation points based on ε.

3.2 Frequency Domain MMSE Equalization with Soft Demodulator

The structure of the frequency domain MMSE equalizer with a soft demodulator is presented in Figure 4. The soft demodulator is used to calculate the log-likelihood ratios for the decoder and the MMSE removes ISI and inter-antenna interference. No IAI suppression is performed in the soft demodulator as the LLRs are calculated separately for each stream. The ith stream of the equalized signal after IDFT can be written as $\mathbf{z}_i = \mathbf{F}_R^{-1}(\mathbf{\Gamma}\mathbf{\Gamma}^{\mathrm{H}} + \sigma^2\mathbf{I})^{-1}\mathbf{\Gamma}_i^{\mathrm{H}}\mathbf{r}$. The equivalent channel for the ith stream $h_{eq} = \frac{1}{K}\mathrm{tr}((\mathbf{\Gamma}_i^{\mathrm{H}}\mathbf{\Sigma}_r^{-1}\mathbf{\Gamma}_i))$ and $\hat{\sigma}_i^2 = h_{eq} - h_{eq}^2$ is the variance of residual interference.

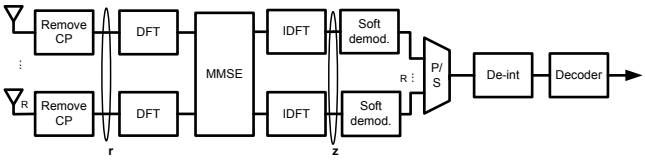

Figure 4: Receiver with soft demodulation.

4. PERFORMANCE COMPARISON

The performances of the algorithms were compared via Monte-Carlo simulations. The MMSE equalizer with soft demodulation from Section 3.2 is denoted in the figures as MMSE. The sphere detectors from Section 3.1 are referred to by the type of tree search used. The turbo receiver is an iterative FD SC-MMSE turbo equalizer with two iterations from [5] in antenna-by-antenna detection mode. The simulation parameters are presented in Table 1. The used channel models are Vehicular A and Pedestrian A [12] and the channel parameters are described in Table 2. The simulations were performed with a single-user MIMO case where both the transmitter and receiver had 4 antennas. The channel was correlated, i.e., there was correlation between the both the transmitter and receiver antennas. The channel correlation is obtained from the antenna azimuth spreads. Simulations were also performed in a virtual MIMO case with four separate 1×4 MIMO channels.

Table 1: Simulation parameters

Coding	3GPP Turbo code
Code rate	1/2 and 2/3
Modulation scheme	64-QAM
Symbol duration	71.4 μs
Channel model	Vehicular A, Pedestrian A

Table 2: Channel model parameters

Number of paths (Veh/Ped)	6/4
Path delays (Veh/Ped)	[0...2510]/[0..410] ns
Path power (Veh/Ped)	[0...−20]/[0...−22.8] dB
BS/MS antenna spacing	4 λ/ 0.5 λ
BS average angle of arrival	50 °
BS/MS azimuth spread	2 °/ 35 °

The performances of the different receivers in a correlated Vehicular A channel are presented in Figure 5 and in a correlated Pedestrian A channel in Figure 6. The simulation results show the FER performance of the single-user

MIMO case and it can be seen that the 2-stage receiver with a time domain sphere detector outperforms the receiver with soft demodulation. With a large delay spread, as in the Vehicular A channel, the difference in performance between the receivers is smaller than that in a channel with smaller delay spread. The equalizer cannot fully suppress the inter-symbol interference (ISI) and this can be seen as degraded performance in the Vehicular A channel case. The difference between receivers is also higher with a larger code rate.

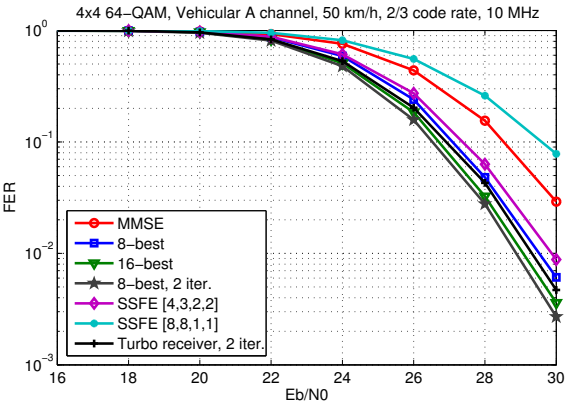

Figure 5: Performance in a correlated Vehicular A channel.

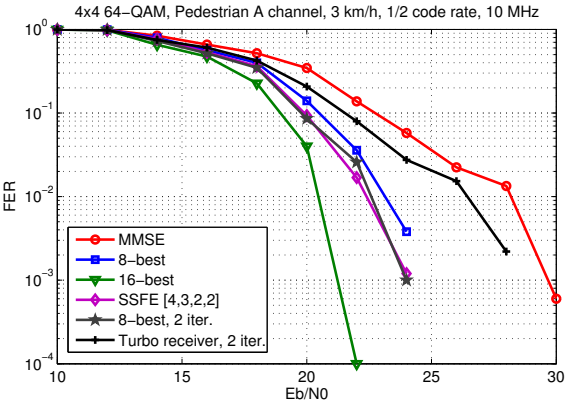

Figure 6: Performance in a correlated Pedestrian A channel.

The performances in a 2×2 MIMO case are presented in Figure 7. A pedestrian A channel was used with a 2/3 code rate. Similar results can be observed as in the 4×4 case except all the tree search algorithms perform similarly. The frequency domain equalizer is not able to suppress the ISI effectively especially in channels with large delay spreads. Therefore, optimizing the MMSE equalizer with additional constraints would be an interesting topic of further study. A time domain sphere detector which would suppress ISI and IAI could also be used to improve the performance but the complexity would be high.

The performances of the receivers in a virtual MIMO scenario are presented in Figure 8 with the Vehicular channel and in Figure 9 with the Pedestrian channel. Without any inter-antenna interference, the ISI dominates the performance. The receivers have similar performances in the Vehicular channel but some performance gain is achieved in the

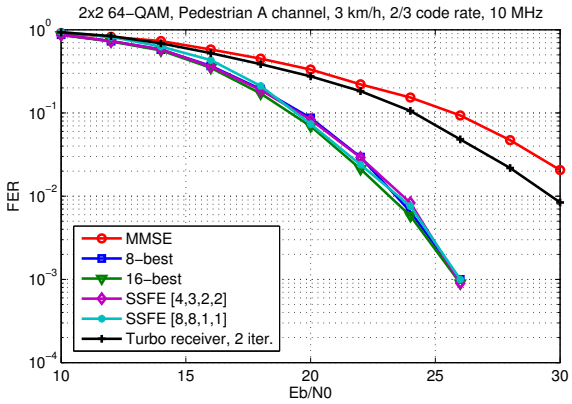

Figure 7: Performance in a correlated 2×2 Pedestrian A channel.

Pedestrian channel with the sphere detectors. The turbo receiver improves the performance especially when there is no IAI. The turbo receiver may not converge in all scenarios depending on the code rate, ISI and IAI even with a high number of iterations. Also the latency may be too high for real time processing. It should be noted that the scenario is not a realistic multi-user scenario but the goal was to simulate the impact of uncorrelated streams on the performance of the receivers.

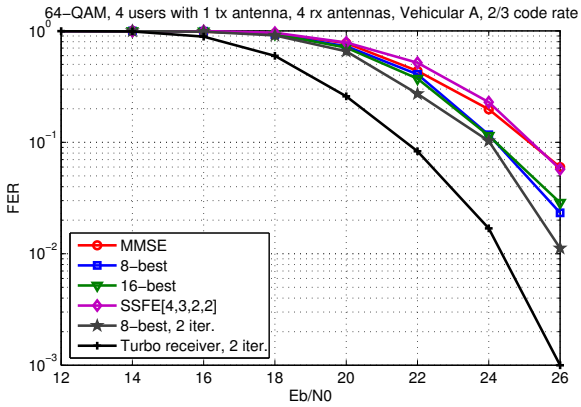

Figure 8: Performance with virtual MIMO in a Vehicular A channel.

5. COMPLEXITY COMPARISON

The complexity of the K-best sphere detector and SSFE in number of multiplications per symbol vector is presented in Table 3 and in Giga operations per second (GOPS) in Table 4. GOPS are defined here as multiplication, comparison and addition operations performed in each algorithm in a 83.3 μs time slot. In the QRD, there are 16.4 MOPS as it only has to be performed once for all subcarriers. The node spanning vectors correspond to those used in the simulations and are [8,8,1,1,1,1,1,1] for SSFE-1 and [4,3,2,2,1,1,1,1] for SSFE-2. The complexity of the soft demodulator for the conventional MMSE receiver is also presented in the table. The high complexity of the soft demodulator comes from the iterations over all the possible transmitted symbol. A look-up

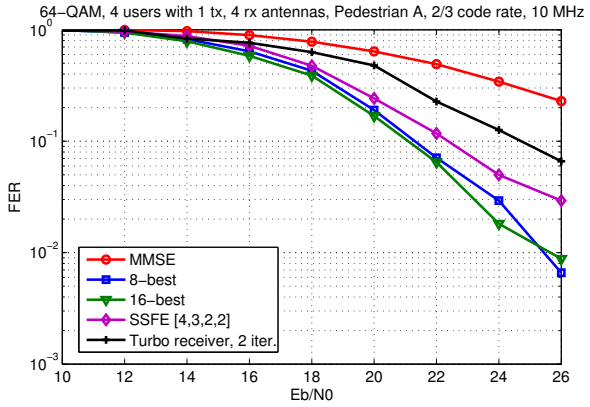

Figure 9: Performance with virtual MIMO in a Pedestrian A channel.

table is also used to calculate a logarithm value. If the look-up table was removed and the LLRs were calculated using a max-log-MAP approximation, the complexity would still be 863.3 GOPS. The soft demodulator also includes a division operation which was approximated here with a multiplication and additions. The soft demodulation could be replaced with a low complexity LLR calculation, where the LLRs are calculated directly from the time domain symbols from the MMSE [13]. This should have only a minor impact on the performance but it was not used the simulations in this paper.

Table 3: Number of multiplication in the detectors

	Multiplications
8-best	1200
16-best	2184
SSFE-1	3105
SSFE-2	2013
Soft demod.	7680
LLR scaling	256

Table 4: Complexity estimates for the time domain processing in GOPS

	Tree search	De-map	LLR	Total
8-best	92.8	7.4	5.9	106.1
16-best	170.6	14.8	11.4	196.8
8-best, 2 it.	92.8	7.4	69.5	169.7
SSFE-1	122.8	59	44.7	226.5
SSFE-2	81.6	44.3	33.65	159.5
Soft demod.				1128.8
LLR scaling				8.6

6. CONCLUSIONS

A 2-stage receiver structure was presented. The sphere detector performed MIMO detection while the MMSE equalizer was used for suppressing ISI and shortening the channel for the sphere detector. Different sphere detection algorithms were compared and some complexity estimates of the time domain detectors were presented. The performance of the proposed receiver was compared to that of the conventional MMSE receiver and it was found to outperform the MMSE receiver. The largest performance gains were observed in the single user MIMO scenario where MIMO detection was needed. The equalizer did not fully suppress the ISI in channels with large delay spreads. Some further optimization could be performed for the equalizer or it could be replaced with an ISI suppressing sphere detector. However, the performance-complexity trade-off of such a detector would require further study.

REFERENCES

[1] 3rd Generation Partnership Project (3GPP); Technical Specification Group Radio Access Network, "Feasibility study for further advancements for E-UTRA (LTE-advanced) (version 9.3.0)," Tech. Rep., 2010.

[2] D. Falconer, S. Ariyavisitakul, A. Benyamin-Seeyar, and B. Eidson, "Frequency domain equalization for single-carrier broadband wireless systems," *IEEE Commun. Mag.*, vol. 40, no. 4, pp. 58–66, 2002.

[3] H. Sari, G. Karam, and I. Jeanclaude, "Frequency domain equalization of mobile radio and terrestrial broadcast channels," in *Proc. IEEE Global Telecommun. Conf.*, 1994, pp. 1 – 5.

[4] M. Tüchler, A. Singer, and R. Koetter, "Minimum mean squared error equalization using a priori information," *IEEE Trans. Signal Processing*, vol. 50, no. 3, pp. 673–683, Mar. 2002.

[5] J. Karjalainen, N. Veselinovic, K. Kansanen, and T. Matsumoto, "Iterative frequency domain joint-over-antenna detection in multiuser MIMO," *IEEE Trans. Wireless Commun.*, vol. 6, no. 10, pp. 3620–3631, Oct. 2007.

[6] M. O. Damen, H. E. Gamal, and G. Caire, "On maximum–likelihood detection and the search for the closest lattice point," *IEEE Trans. Inform. Theory*, vol. 49, no. 10, pp. 2389–2402, Oct. 2003.

[7] B. Hochwald and S. ten Brink, "Achieving near-capacity on a multiple-antenna channel," *IEEE Trans. Commun.*, vol. 51, no. 3, pp. 389–399, Mar. 2003.

[8] M. Myllylä, M. Juntti, and J. Cavallaro, "Implementation aspects of list sphere decoder algorithms for MIMO-OFDM systems," *Elsevier Journal on Signal Processing*, vol. 90, no. 10, pp. 2863–2876, 2010.

[9] J. Ketonen, M. Juntti, and J. Cavallaro, "Performance-complexity comparison of receivers for a LTE MIMO-OFDM system," *IEEE Trans. Signal Processing*, vol. 58, no. 6, pp. 3360–3372, Jun. 2010.

[10] K. Wong, C. Tsui, R. K. Cheng, and W. Mow, "A VLSI architecture of a K-best lattice decoding algorithm for MIMO channels," in *Proc. IEEE Int. Symp. Circuits and Systems*, vol. 3, Scottsdale, AZ, May 26-29 2002, pp. 273–276.

[11] M. Li, B. Bougart, E. Lopez, and A. Bourdoux, "Selective spanning with fast enumeration: A near maximum-likelihood MIMO detector designed for parallel programmable baseband architectures," in *Proc. IEEE Int. Conf. Commun.*, Beijing, China, May19-23 2008, pp. 737 – 741.

[12] 3rd Generation Partnership Project (3GPP); Technical Specification Group Radio Access Network, "Spatial channel model for multiple input multiple output (MIMO) simulations (3G TS 25.996 version 7.0.0 (release 7))," 3rd Generation Partnership Project (3GPP), Tech. Rep., 2007.

[13] I. Collings, M. Butler, and M. McKay, "Low complexity receiver design for MIMO bit-interleaved coded modulation," in *Proc. IEEE Int. Symp. Spread Spectrum Techniques and Applications*, Sydney, Australia, Aug. 30 – Sep. 2 2004, pp. 1993–1997.